Mathematical Theory and Modeling
ISSN 2224-5804 (Paper) ISSN 2225-0522 (Online)
Vol.5, No.5, 2015

Effect of Peak Temperature on Biomass Pyrolysis Characteristics in Thermally Thin Regime in a Fixed-Bed Reactor

Pious O. Okekunle

Department of Mechanical Engineering, Faculty of Engineering and Technology,
Ladoke Akintola University of Technology, P.M.B. 4000, Ogbomoso, Oyo state, Nigeria.

Author's email address: pookekunle@lautech.edu.ng

Abstract

Effect of reactor peak temperature on biomass pyrolysis in thermally thin regime with a constant heating rate of 30 K/s, reactor pressure of 1 atm and reactor peak temperature ranging from 500 to 1000 ^{o}C in a fixed-bed reactor has been numerically investigated. Wood samples ($\rho = 400\ kg/m^3$, $\emptyset\ 1\ mm$ and length $1\ mm$) were modeled as two-dimensional porous solids. Transport equations, solid mass conservation equations, intra-particle pressure generation equation and energy conservation equation were coupled and simultaneously solved to simulate the pyrolysis process. First order Euler Implicit Method (EIM) was used to solve the solid mass conservation equations. The transport, energy conservation and intra-particle pressure generation equations were discretized by Finite Volume Method (FVM). The generated set of linear equations was solved by Tri-Diagonal Matrix Algorithm (TDMA). Intra-particle fluid flow velocity was estimated by Darcy's law. Results showed that increase in reactor peak temperature from 500 to 600 ^{o}C slightly increased the degree of volatiles intra-particle secondary reactions and that further increase of the former has no effect on the latter. Increasing reactor peak temperature from 500 to 600 ^{o}C also resulted in slight increase in gas and secondary tar yield but some decrease in tar and char yield. Further increase in reactor peak temperature above 600 ^{o}C has no effect on products evolution and yields. The highest tar yield (45.31%) was obtained at 500 ^{o}C.

Keywords: Biomass, pyrolysis, intra-particle secondary reactions, thermally thin regime

1. Introduction

For decades, several attempts have been made in order to devise renewable sources of energy for sustainable development. This resulted from the depletion of conventional fossil fuel resources and environmental impacts of burning fossils. Amongst various renewable energy options, biomass technology is gaining attention. To optimize reactor design and biomass thermochemical conversion systems, a better understanding of the influence of process parameters on pyrolysis characteristics is of prime importance. Many research works have been done in this area [1-10]. It has been reported that particle sizes for fast pyrolysis aimed at liquid fuel production are in the range 0.1 – 6 mm [11-12] with reactor temperature roughly between 700 and 800 K. Recently, we have studied the effect of pyrolysis pressure on biomass pyrolysis characteristics in thermally thin regime [13]. We have also studied the combined effect of pressure and heating rate on biomass pyrolysis product distribution [14]. Although many researchers have studied the effect of temperature on biomass pyrolysis [15-17], very few have attempted to clarify the mechanism of intra-particle secondary reactions of volatiles (mainly tar) during the process. Therefore, in this study, the influence of final reactor temperature on pyrolysis characteristics in thermally thin regime was investigated with emphasis on evolution patterns of gas and tar, quantification of the extent of primary tar intra-particle secondary reactions and the final yields of products. The implications of these results were also discussed**.**

2. Pyrolysis Mechanism

Figure 1 shows the structure of the pyrolysis mechanism adopted in this study. A detailed explanation on the development of this mechanism has been reported in our earlier research works [18, 19]. As shown in the figure, wood first decomposes by three endothermic competing primary reactions to form gas, primary tar and intermediate solid. The primary tar undergoes secondary reactions to yield more gas and char. The intermediate

solid is further transformed into char by a strong exothermic reaction as shown in the figure. Reaction rates were assumed to follow Arrhenius expression of the form; $k_i = A_i \exp\left(-E_i/RT\right)$. The chemical kinetic (*A* and *E*) and thermodynamic (*a* and *b*) parameters are as given in one of our previous works [19].

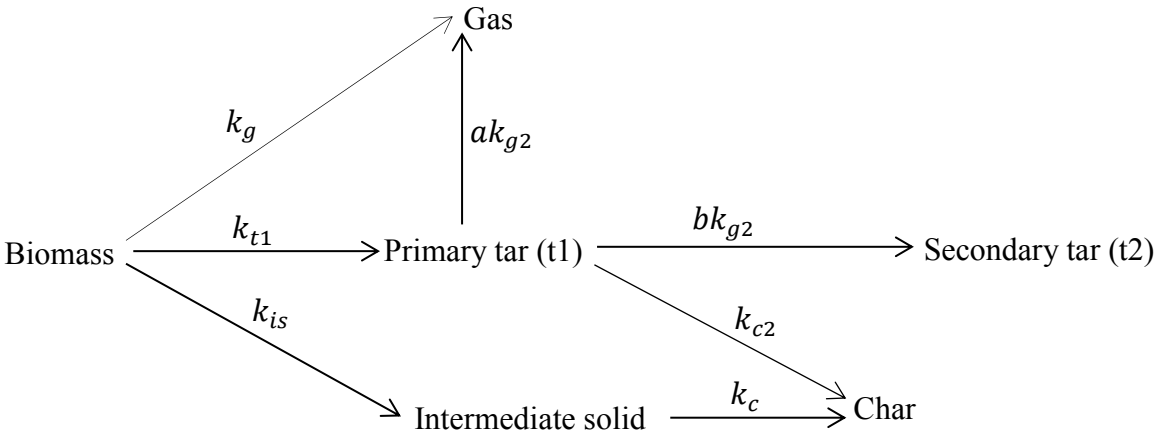

Figure 1: Schematic illustration of pyrolysis mechanism

3. Numerical simulation

The governing equations, model assumptions and numerical procedures in this study are already given in our previous studies [18, 19, 20]. Hence, fundamental governing equations will only be set out.

3.1 Solid mass conservation equation

The instantaneous mass balance of the pyrolyzing solid comprises three endothermic consumption terms yielding gas, primary tar and intermediate solid:

$$\frac{\partial \rho_s}{\partial t} = -(k_g + k_t + k_{is})\rho_s \quad (1)$$

The intermediate solid instantaneous mass balance equation (equation (2)) contains two terms, one for the conversion of the virgin solid to intermediate solid and the other from exothermic decomposition of intermediate solid to yield char, given as

$$\frac{\partial \rho_{is}}{\partial t} = k_{is}\rho_s - k_c\rho_{is} \quad (2)$$

Also, the char instantaneous mass balance equation (equation(3)) contains two terms, one from the exothermic decomposition of intermediate solid and the other from primary tar secondary reaction to yield char, given as

$$\frac{\partial \rho_c}{\partial t} = k_c\rho_{is} + k_{c2}\rho_t \quad (3)$$

3.2 Mass conservation equations of gas phase components

Mass conservation equations for all gas phase components are expressed by two-dimensional cylindrical coordinate system consisting of both temporal and spatial gradients and source terms, given by

$$\text{Ar: } \frac{\partial(\varepsilon\rho_{Ar})}{\partial t} + \frac{\partial(\rho_{Ar}U)}{\partial z} + \frac{1}{r}\frac{\partial(r\rho_{Ar}V)}{\partial r} = S_{Ar}, \quad (4)$$

$$\text{Gas: } \frac{\partial(\varepsilon\rho_g)}{\partial t} + \frac{\partial(\rho_g U)}{\partial z} + \frac{1}{r}\frac{\partial(r\rho_g V)}{\partial r} = S_g, \quad (5)$$

Primary tar : $\frac{\partial(\varepsilon\rho_{t1})}{\partial t}+\frac{\partial(\rho_{t1}U)}{\partial z}+\frac{1}{r}\frac{\partial(r\rho_{t1}V)}{\partial r}=S_{t1},$ (6)

Secondary tar: $\frac{\partial(\varepsilon\rho_{t2})}{\partial t}+\frac{\partial(\rho_{t2}U)}{\partial z}+\frac{1}{r}\frac{\partial(r\rho_{t2}V)}{\partial r}=S_{t2}$ (7)

S_{Ar} , S_g, S_{t1} and S_{t2} are the source terms for the carrier gas (argon), gas, primary tar and secondary tar respectively, and are given by

$S_{Ar}=0$ (8)

$S_g=k_g\rho_s+\varepsilon k_{g2}\rho_{t1}$ (9)

$S_{t1}=k_t\rho_s-\varepsilon[k_{c2}+(a+b)k_{g2}]\rho_{t1}$ (10)

$S_{t2}=\varepsilon bk_{g2}\rho_{t1}$ (11)

Intra-particle tar and gas transport velocity was estimated by Darcy's law, expressed as

$U=-\frac{B}{\mu}\left(\frac{\partial P}{\partial z}\right)$ (12)

$V=-\frac{B}{\mu}\left(\frac{\partial P}{\partial r}\right)$ (13)

where B and μ are respectively the charring biomass solid permeability and kinematic viscosity. Porosity, ε, is expressed as

$\varepsilon=1-\frac{\rho_{s,sum}}{\rho_{w,0}}(1-\varepsilon_{w,0})$ (14)

where $\varepsilon_{w,0}$, $\rho_{s,sum}$ and $\rho_{w,0}$ are the initial porosity of wood, the sum of solid mass density and initial wood density, respectively. The permeability, B, of the charring biomass is expressed as a linear interpolation between the solid phase components, given as

$B=(1-\eta)B_w+\eta B_c$ (15)

where η is the degree of pyrolysis and is defined as

$\eta=1-\frac{\rho_s+\rho_{is}}{\rho_{w,0}}$ (16)

3.3 Energy conservation equation

The energy conservation equation is given as

$$\left(C_{p,w}\rho_s+C_{p,w}\rho_{is}+C_{p,c}\rho_c+\varepsilon C_{p,t}\rho_{t1}+\varepsilon C_{p,t}\rho_{t2}+\varepsilon C_{p,g}\rho_g\right)\frac{\partial T}{\partial t}=\frac{\partial}{\partial z}\left(k_{eff(z)}\frac{\partial T}{\partial z}\right)+\frac{1}{r}\frac{\partial}{\partial r}\left(rk_{eff(r)}\frac{\partial T}{\partial r}\right)-l_c\Delta h_c-\sum_{i=g,t1,is}m_i\Delta h_i-\varepsilon\sum_{i=g2,t2,c2}n_i\Delta h_i \quad (17)$$

where

$l_c=A_c\exp(-E_c/RT)\,\rho_{is}$ (18)

$m_i=A_i\exp(-E_i/RT)\,\rho_s \quad i=g,t1,is$ (19)

$n_i=A_i\exp(-E_i/RT)\,\rho_{t1} \quad i=g2,t2,c2$ (20)

The thermo-physical properties of the wood sample are as given in our previous study [13].

3.4 Pressure evolution

The total pressure is the sum of the partial pressures of the inert gas (argon), gas and secondary tar from the pyrolysis process. It is given as

$$P = P_{Ar} + P_{t2} + P_g;\ \ P_i = \frac{\rho_i RT}{M_i} \qquad (i = Ar, t2, g) \tag{21}$$

where M_i and R are the molecular weight of each gaseous species and universal gas constant, respectively. Combining equations (4), (5), (7), (12), (13) and (21), intra-particle pressure equation was obtained as

$$\frac{\partial}{\partial t}\left(\varepsilon \frac{P}{T}\right) - \frac{\partial}{\partial r}\left[\frac{BP}{\mu T}\left(\frac{\partial P}{\partial z}\right)\right] - \frac{1}{r}\frac{\partial}{\partial r}\left[r\frac{BP}{\mu T}\left(\frac{\partial P}{\partial r}\right)\right] = \frac{R}{M_{t2}}S_{t2} + \frac{R}{M_g}S_g \tag{22}$$

3.5 Numerical Procedure

Wood pellets were modeled as two-dimensional porous solids. Wood pores were assumed to be initially filled with argon. As the solid was pyrolyzed, tar and gas were formed while argon was displaced to the outer region without participating in the pyrolysis reaction. The solid mass conservation equations (eqs (1) – (3)) were solved by first-order Euler Implicit Method. The mass conservation equations for argon, primary tar, gas and secondary tar (eqs (4) – (7)), energy conservation equation (eq. (17)) and the pressure equation (eq. (22)) were discretized using Finite Volume Method (FVM). Hybrid differencing scheme was adopted for the convective terms. First-order fully implicit scheme was used for the time integral with time step of 0.005 s. The detailed numerical procedure and calculation domain have been given somewhere else [18]. Model assumptions have also been given previously [20].

4. Results and discussion

4.1 Effect on weight loss history

Figure 2 shows the weight loss history of the pyrolyzing solid for different final reactor temperature considered (500, 600, 700, 800, 900 and 1000 ^{o}C). From the figure, it is clearly seen that sample heating continued until about 8 s when active disintegration of the pyrolyzing sample commenced for all the reactor temperature considered. This implies that the rate of biomass conversion at the initial stage of the process was not significantly different for all the peak reactor temperatures. This is understandable from the fact that some time is required for the furnace to attain the final temperature from initial temperature of 187 ^{o}C. At 12 s, the weight loss profile at reactor peak temperature of 500 ^{o}C began to be less steep than at other higher temperature until the process got terminated at about 15 s. This may be due to the fact that as the final reactor temperature increases, the rate of heat transfer from the reactor ambient and the pyrolyzing solid increases thereby accelerating the rate of biomass conversion to gas, tar and char. This difference in weight loss history widened with time until the process is terminated when the peak temperature of 500 ^{o}C was reached at about 15 s. At peak temperature of 600 ^{o}C and above, there was no significant difference in the weight loss history. This may be due to the fact that biomass conversion to various products was almost completed before the reactor ambient reached 600 ^{o}C and as a result brought no significant changes in sample weight loss pattern even at temperatures higher than 600 ^{o}C.

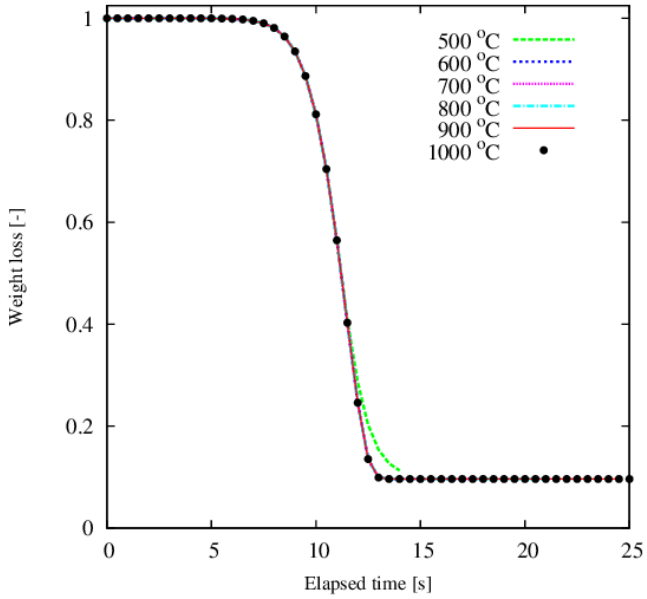

Figure 2: Weight loss history at different reactor peak temperatures

4.2 Effect on primary tar evolution

Figure 3 shows the rate of primary tar production at various pyrolysis temperatures. From the figure, the primary tar production rate at 500 °C was similar to the rates at higher temperatures (600 – 1000 °C) as the later rises until it got to its peak at about 11 s. After reaching the peak, primary tar production rate at 500 °C began to fall as a result of the fact that much of the sample has already been converted and rate of primary tar production has now begun to decrease. This continued until pyrolysis was terminated at about 14 s (Figure 2). As seen from the figure, primary tar production rates from 600 °C to 1000 °C increased following the same trend and were similar to that at 500 °C except for higher peaks reached almost within the same time frame. This probably was due to a higher thermal flux the sample was subjected to at 600 °C and above. Furthermore, it could also be seen from the figure that primary tar production rates at 600 °C and above also began to decline having reached their peaks, the slopes of decline being steeper than that at 500 °C. The reason for this scenario has already been given earlier.

4.3 Effect on secondary reactions products generation

Figure 4 shows the rate of products generation from intra-particle secondary reactions at different temperature. From the figure, products generation profiles were the same from 600 °C to 1000 °C , with much higher peaks than at 500 °C. This was as a result of the fact that at 600 °C and above, exposure of the pyrolyzing solid to a higher thermal flux favoured intra-particle secondary reactions thereby yielding more secondary products. Other researchers have found that from 600 °C and above, tar cracking is favoured during pyrolysis [21]. In this study, primary tar secondary reactions are considered to yield secondary tar, more gas and char (Figure 1). The detailed explanation of this primary tar secondary reactions mechanism has been given previously [19].

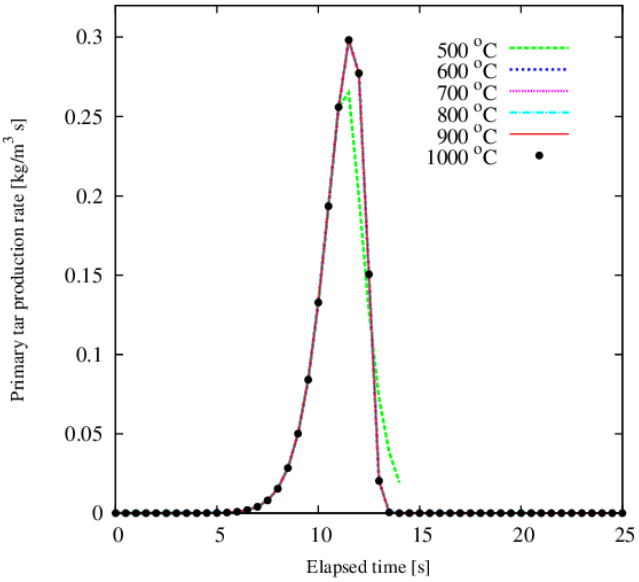

Figure 3: Primary tar production rate at different reactor peak temperatures

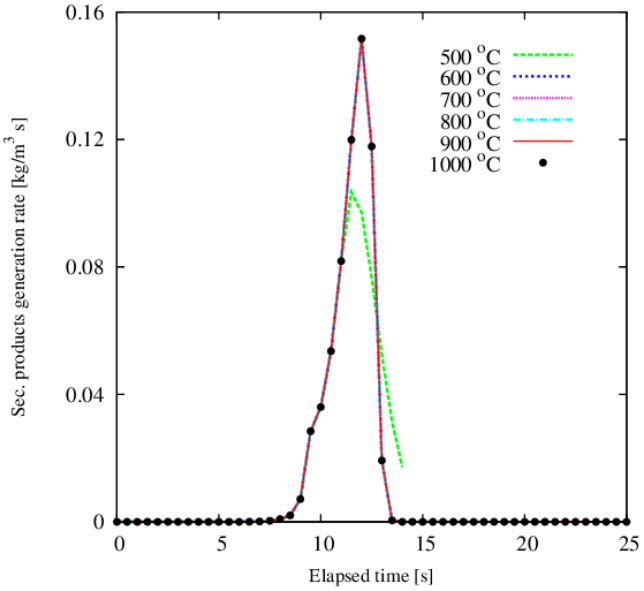

Figure 4: Secondary products generation rates at different reactor peak temperatures

4.4 Effect on primary tar release rate

Figure 5 shows primary tar release rates at different temperatures. From the figure, for all temperatures considered, there was no significant release of tar until about 6 s. Earlier than this time, the heat supplied to the pyrolyzing sample was used to raise its temperature to a value sufficient to initiate biomass decomposition. The trend of primary tar release rates for all reactor peak temperatures considered were similar till about 11 s. The peak primary tar release profile at 600 ^{o}C was however slightly higher than at 500 ^{o}C. Further increase in reactor peak temperature did not have any significant effect on tar release rate and from 600 ^{o}C to 1000 ^{o}C, the peaks of all profiles were the same. There are two reasons to justify this. In the first place, in thermally thin regime, volatile residence time within the sample is so short that intra-particle secondary reactions are limited. Secondly, considering the size of the sample, much of the sample would have been converted or decomposed to other products at 600 ^{o}C, hence no significant decomposition took place even though the reactor temperature rose beyond this temperature.

4.5 Effect on gas release rate

Figure 6 shows the rates of gas release at different reactor temperatures. From the figure, the peaks of gas release rates profiles from 600 ^{o}C to 1000 ^{o}C were the same and were higher than at 500 ^{o}C. Besides, as the profiles declined after reaching their peaks, the declination slope at 600 ^{o}C and above was steeper that at 500 ^{o}C, the reason being that at higher temperatures than 500 ^{o}C, the rate of biomass decomposition was higher and intra-particle secondary reactions were also enhanced, thereby resulting in drastic reduction in the rate of gas release with time.

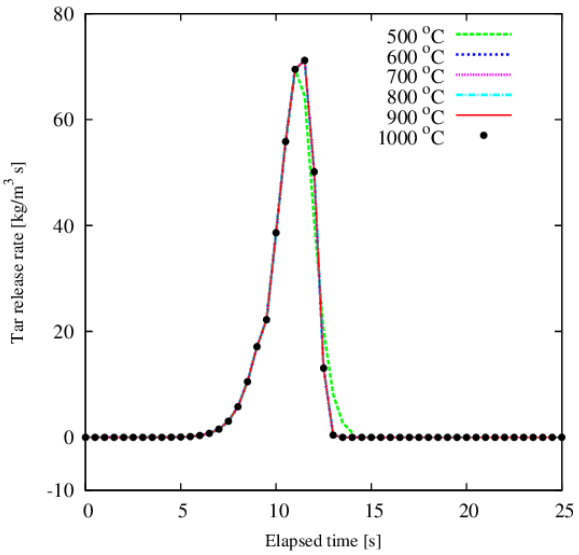

Figure 5: Primary tar release rates at different reactor peak temperatures

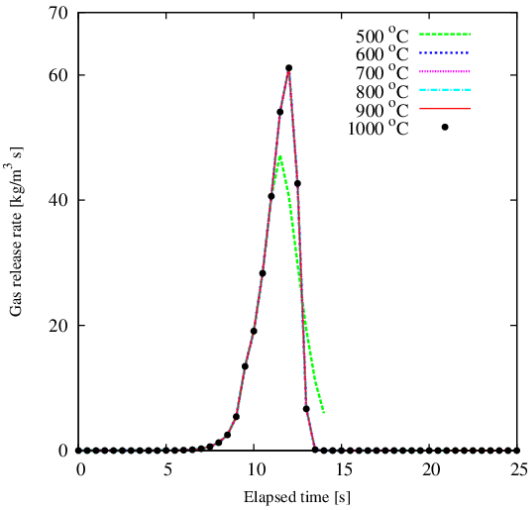

Figure 6: Gas release rates at different reactor peak temperatures

4.6 Effect on intra-particle secondary reactions

For a better understanding of the influence of reactor peak temperature on intra-particle secondary reactions in thermally thin regime, the ratio of the rate of secondary reactions products generation (R_s) to the rate of primary tar production (R_p) for each reactor temperature was calculated. Figure 7 shows R_s/R_p at different reactor temperatures. From the figure, the ratio R_s/R_p increased from 0.39 to 0.408 as reactor temperature increased from 500 to 600 ^oC. Further increase in the reactor temperature did not have any significant effect on this ratio. This implies that in the thermally thin regime, intra-particle secondary reactions may have no significant effects on pyrolysis products distribution and yield at temperature above 600 ^oC.

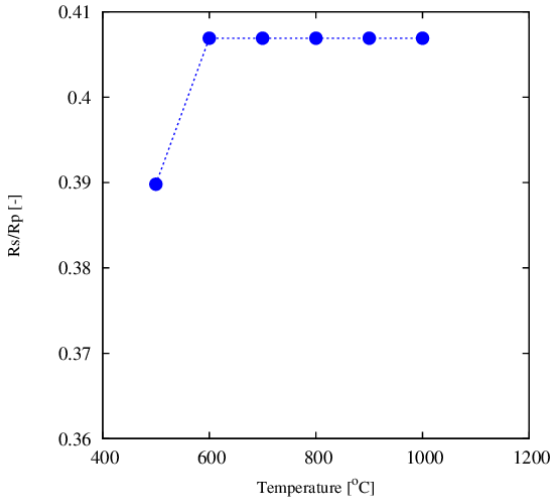

Figure 7: The ratio of the rate of primary tar secondary reactions products generation to the rate of primary tar production at different reactor peak temperatures

4.7 Total product yields

Figure 8 shows the total yield of product species at different reactor temperatures. From the figure, as the reactor temperature increased from 500 to 600 ^{o}C, gas and secondary tar yield increased slightly while char yield decreased.

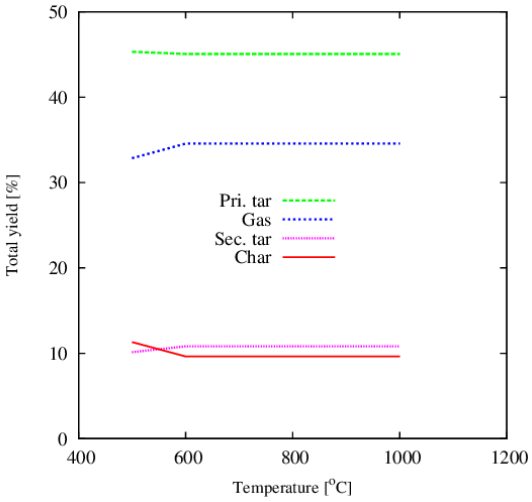

Figure 8: Product yield at different reactor peak temperatures

With temperature increase from 500 to 600 ^{o}C, although there was a light decrease in tar yield (0.25%), this decrease was hard to observe in Figure 8. For all the product species, further increase in temperature above 600 ^{o}C had no effect on the total yield. As explained earlier, considering the size of the particle, the residence time of the volatiles within the pyrolyzing solid was so short that intra-particle secondary reactions could not take place significantly. Furthermore, biomass decomposition was almost complete before the reactor attained the peak temperature (just within 14 s). These are plausible reasons for these results. The highest yield of tar, also referred to as bio-oil, (45.31%) was obtained at 500 ^{o}C. These results are in agreement with the recent findings of some other researchers [22].

5. Conclusions

Influence of reactor peak temperature on primary tar intra-particle secondary reactions, product evolution and total yields during biomass pyrolysis has been investigated in a thermally thin regime and under a constant heating rate of 30 K/s with reactor peak temperature ranging from 500 to 1000 ^{o}C in a fixed bed reactor. Results revealed that increase in peak temperature of the reactor did not significantly influence volatiles intra-particle secondary reactions. Findings also showed that product evolution and yields from 600 to 1000 ^{o}C were similar. The highest yield of bio-oil was obtained at 500 ^{o}C. In fast pyrolysis processes, where optimum yield of liquid is desired, average temperature in the neighbourhood of 500 to 600 ^{o}C may be appropriate.

Nomenclature

A: pre-exponential factor	(1/s)
B: permeability	(m^2)
Cp: specific heat capacity	(J/ kg K)
E: activation energy	(J/mol)
e: emissivity	(-)

h_c: convective heat transfer coefficient	(W/ m^2 K)
k: reaction rate constant	(1/s)
k_c: char thermal conductivity	(W/m K)
k_w: wood thermal conductivity	(W/m K)
M: molecular weight	(kg/mol)
P: Pressure	(Pa)
Q: heat generation	(W/m^3)
Q_c: convective heat flux	(W/m^2)
Q_r: radiation heat flux	(W/m^2)
R: universal gas constant	(J/mol K)
R: total radial length	(m)
r: radial direction	
z: axial direction	
S: source term	
T: temperature	(K)
t : time	(s)
U: axial velocity component	(m/s)
V: radial velocity component	(m/s)
ε: porosity	(-)
ε_0: initial porosity	(-)
Δh: heat of reaction	(kJ/kg)
μ: viscosity	(kg/m s)
ρ: density	(kg/m^3)
ρ_{w0}: initial density of wood	(kg/m^3)
σ: Stefan-Boltzmann constant	($W/m^2 K^4$)
η: degree of pyrolysis	

Subscripts
Ar: Argon
c: char, primary char formation reaction
c_2: secondary char formation reaction
g: gas, primary gas formation reaction
g_2: secondary gas formation reaction
is: intermediate solid, intermediate solid formation reaction
s: solid
t: tar, tar formation reaction
v: total volatile
w: wood

References

[1] Horne, P.A. & Williams, P.T. (1996). Influence of Temperature on the Products from the Flash Pyrolysis of Biomass. *Fuel*, 75, 1051-1059.
[2] Antal, M.J., Mochidzuki, K. & Paredes, L.S. (2003). Flash carbonization of Biomass. *Industrial Engineering Chemistry Research*, 42, 3690-3696. In Modeling Chemical and Physical processes of Wood and Biomass Pyrolysis,Progress in Energy and Combustion Science, 34 (2008), 47-90.
[3] Okekunle, P.O., Watanabe, H. & Okazaki, K. (2013). Analysis of Biomass Pyrolysis Product Yield Distribution in Thermally Thin Regime at Different Heating Rates. *Mathematical Theory and Modeling* **3**(11), 28-34.
[4] Antal, M.J. (1983). Effects of Reactor Severity on the Gas-phase Pyrolysis of cellulose and Kraft Lignin-derived Volatile Matter. *Industrial Engineering Production Research and Development*, 22, 366-375.
[5] Miller, R.S. & Bellan, J. (1996) Analysis of Reaction Products and Conversion Time in the Pyrolysis of Cellulose and Wood particles, *Combustion Science and Technology*, 119, 331-373.
[6] Shuangning, X., Zhihe, L., Baoming, L., Weiming, Y. & Xueyuan, B. (2006) Devolatilization Characteristics of Biomass at Flash Heating Rate. *Fuel*, 85: 664-670.
[7] Guo, X., Xu, Y., Yang, X. & Qin, F.G.F. (2014) Effect of Heating Rate on Edible Mushroom Bran Pyrolysis. *Energy Procedia*, 61: 533-537.
[8]Authier, O. & Lédé, J. (2014) Temperature and Heating Rate of Solid Particles Undergoing Thermal Decomposition. Which Criteria for Characterizing Fast Pyrolysis? *Journal of analytical and Applied Pyrolysis*. In Press, http://dx.doi.org/10.1016/j.jaap.2014.11.013.

[9] Efika, E.C., Onwudili, J.A. & Williams, P.T. (2015) Products from the High Temperature Pyrolysis of RDF at Slow and Rapid Heating Rates. *Journal of Analytical and Applied Pyrolysis*, 112:14-22.
[10] Liaw, S., Wang, Z., Ndegwa, P., Frear, C., Ha, S. & Li, C. (2012) Effect of Pyrolysis Temperature on the Yield and Properties of Bio-Oils Obtained from the Auger Pyrolysis of Douglas Fir Wood. *Journal of Analytical and Applied Pyrolysis*, 93: 52-62.
[11] Bridgwater, A.V. (1999) Principles and Practice of Biomass Fast Pyrolysis Processes for Liquids. *Journal of Analytical and Applied Pyrolysis*, 51: 3-22. In: Di Blasi, C. (2002) Modeling Intra- and Extra-Particle Processes of Wood Fast Pyrolysis. *AIChE Journal*, 48(10): 2386 – 2397.
[12] Scott, D.S., Majerski, P., Piskorz, J. & Radlein, D. (1999) A Second Look at Fast Pyrolysis of Biomass – The RTI Process, Journal of Analytical and Applied Pyrolysis, 51: 23-37. In: Di Blasi, C. (2002) Modeling Intra- and Extra-Particle Processes of Wood Fast Pyrolysis. *AIChE Journal*, 48(10): 2386 – 2397.
[13] Okekunle, P.O. & Osowade E.A. (2014). Numerical Investigation of the Effects of Reactor Pressure on Biomass Pyrolysis in Thermally Thin Regime. *Journal of Chemical and Process Engineering Research*, 27, 12-22.
[14] Okekunle, P.O., Osowade, E.A. & Oyekale, J.O. (2015) Numerical Investigation of the Combined Impact of Reactor Pressure and Heating Rate on Evolution and Yields of Biomass Pyrolysis Products in Thermally Thin Regime, *Journal of Energy Technologies and Policies*, 5(3), 93-106.
[15] Gómez, N., Rosas, J.G., Cara, J., Martínez, O., Alburquerque, J.A. & Sánchez, M.E. (2014) Slow Pyrolysis of Relevant Biomasses in the Mediterranean Basin. Part 1. Effect of Temperature on Process Performance on a Pilot Scale. *Journal of Cleaner Production*, In Press: http://dx.doi.org/10.1016/j.jclepro.2014.10.082.
[16] Yang, H., Yan, R., Chen, H., Lee, D.H., Liang, D.T. & Zheng, C. (2006). Pyrolysis of palm oil wastes for enhanced production of hydrogen rich gases. *Fuel Processing Technology*. 87: 935–942.
[17] Yang, H., Yan, R., Chen, H., Lee, D.H.& Zheng, C. (2007) Characteristics of Hemicellulose, Cellulose and Lignin Pyrolysis. *Fuel*. 86: *1781 – 1788.*
[18] Okekunle, P.O., Watanabe, H., Pattanotai, T. & Okazaki, K. (2012). Effect of Biomass Size and Aspect Ratio
on Intra-particle Tar Decomposition during Wood Cylinder Pyrolysis. *Journal of Thermal Science and Technology* 7(1), 1-15.
[19] Okekunle, P.O., Pattanotai, T., Watanabe, H. & Okazaki, K. (2011). Numerical and Experimental Investigation of Intra-particle Heat Transfer and Tar Decomposition during Pyrolysis of Wood Biomass. *Journal of Thermal Science and Technology*, 6(3), 360-375.
[20] Okekunle, P.O. (2013) Numerical Investigation of the Effects of Thermo-physical Properties on Tar Intra-particle Secondary Reactions during Biomass Pyrolysis, *Mathematical Theory and Modeling*, 3(14), 83-97.
[21] Fagbemi, L., Khezami, L. and Capart, R. (2001). Pyrolysis from Different Biomasses: Application to the Thermal Cracking of Tar. *Applied Energy*, 69, 293-306.
[22] Aysu, T. & Küçük, M.M. (2014) Biomass Pyrolysis in a Fixed-Bed Reactor: Effects of Pyrolysis Parameters on Product Yields and Characterization of Products. *Energy*, 64, 1002-1025.

The IISTE is a pioneer in the Open-Access hosting service and academic event management. The aim of the firm is Accelerating Global Knowledge Sharing.

More information about the firm can be found on the homepage:
http://www.iiste.org

CALL FOR JOURNAL PAPERS

There are more than 30 peer-reviewed academic journals hosted under the hosting platform.

Prospective authors of journals can find the submission instruction on the following page: http://www.iiste.org/journals/ All the journals articles are available online to the readers all over the world without financial, legal, or technical barriers other than those inseparable from gaining access to the internet itself. Paper version of the journals is also available upon request of readers and authors.

MORE RESOURCES

Book publication information: http://www.iiste.org/book/

Academic conference: http://www.iiste.org/conference/upcoming-conferences-call-for-paper/

IISTE Knowledge Sharing Partners

EBSCO, Index Copernicus, Ulrich's Periodicals Directory, JournalTOCS, PKP Open Archives Harvester, Bielefeld Academic Search Engine, Elektronische Zeitschriftenbibliothek EZB, Open J-Gate, OCLC WorldCat, Universe Digtial Library , NewJour, Google Scholar